Front. Earth Sci. 2022, 16(1): 90–98
https://doi.org/10.1007/s11707-021-0887-8

RESEARCH ARTICLE

High-resolution sea surface wind speeds of Super Typhoon Lekima (2019) retrieved by Gaofen-3 SAR

He FANG[1,2], William PERRIE[4], Gaofeng FAN[1], Zhengquan LI[1], Juzhen CAI[1], Yue HE[1], Jingsong YANG[2], Tao XIE[5], Xuesong ZHU (✉)[3]

1 Zhejiang Climate Centre, Hangzhou 310017, China
2 State Key Laboratory of Satellite Ocean Environment Dynamics, Second Institute of Oceanography, Ministry of Natural Resources, Hangzhou 310012, China
3 Shanghai Typhoon Institute, and Key Laboratory of Numerical Modeling for Tropical Cyclone of China Meteorological Administration, Shanghai 200030, China
4 Fisheries & Oceans Canada, Bedford Institute of Oceanography, Dartmouth B2Y4A2, Canada
5 School of Remote Sensing and Geomatics Engineering, Nanjing University of Information Science and Technology, Nanjing 210044, China

Abstract Gaofen-3 (GF-3) is the first Chinese spaceborne multi-polarization synthetic aperture radar (SAR) instrument at C-band (5.43 GHz). In this paper, we use data collected from GF-3 to observe Super Typhoon Lekima (2019) in the East China Sea. Using a VH-polarized wide ScanSAR (WSC) image, ocean surface wind speeds at 100m horizontal resolution are obtained at 21:56:59 UTC on 8 August 2019, with the maximum wind speed, 38.9 $m \cdot s^{-1}$. Validating the SAR-retrieved winds with buoy-measured wind speeds, we find that the root mean square error (RMSE) is 1.86 $m \cdot s^{-1}$, and correlation coefficient, 0.92. This suggests that wind speeds retrieved from GF-3 SAR are reliable. Both the European Centre for Medium-Range Weather Forecasts (ECMWF) fine grid operational forecast products with spatial resolution, and China Global/Regional Assimilation and Prediction Enhance System (GRAPES) have good performances on surface wind prediction under weak wind speed condition (< 24 $m \cdot s^{-1}$), but underestimate the maximum wind speed when the storm is intensified as a severe tropical storm (> 24 $m \cdot s^{-1}$). With respect to SAR-retrieved wind speeds, the RMSEs are 5.24 $m \cdot s^{-1}$ for ECMWF and 5.17 $m \cdot s^{-1}$ for GRAPES, with biases of 4.16 $m \cdot s^{-1}$ for ECMWF and 3.84 $m \cdot s^{-1}$ for GRAPES during Super Typhoon Lekima (2019).

Keywords synthetic aperture radar, wind speed, numerical weather predication (NWP), typhoon

Received September 17, 2020; accepted January 20, 2021

E-mail: zhuxs@typhoon.org.cn

1 Introduction

Typhoons (known as hurricanes in the Atlantic) are associated with heavy rain, flooding and coastal inundation, and represent some of the most expensive and dangerous natural disasters for coastal countries. The forecasting of ocean surface winds under typhoon conditions is quite challenging, because measurements are difficult to acquire. The 2-min mean maximum wind speed (MWS) defines the typhoon's intensity (Uhlhorn et al., 2014). However, for practical purposes, monitoring the entire typhoon wind field is perhaps more important, for example as quantified by the integrated kinetic energy (Buchanan et al., 2018). Accurate estimates of typhoon winds play an important role in early warning, forecasting and mitigation of typhoon disasters.

The satellite-based Dvorak technique is the main tool that is readily available and widely applied around the world for making operational estimates of typhoon intensity, defined as the maximum sustained surface wind speeds. It is based on assessments of satellite imagery (enhanced infrared or visible) and an established rule-based methodology (Cangialosi et al., 2015). Over the last 30 years, a large dataset of typhoon characteristics has become available, especially for cases of rapid intensification. However, large departures in the typhoon intensity estimates often occur between different agencies, using the same Dvorak technique. It is likely that lack of observations in the open ocean may contribute to this lack of agreement (Sangster and Landsea, 2020). Recently, using the data collected from typhoon intensity official forecasts issued by the China Meteorological Administration (CMA), the Joint Typhoon Warning Center (JTWC) and

the Regional Specialized Meteorological Center Tokyo-Typhoon Center (RSMC-Tokyo), Huang et al. (2021) systematically evaluates the accuracy for western North Pacific tropical cyclone intensity forecasts between 2005 and 2018. The results show that the JTWC had the highest accuracy at 24 h – 120 h. At 24 h and 48 h, the accuracy of the RSMC-Tokyo was higher than that of the CMA. At 72 h, the CMA's accuracy exceeded that of the RSMC-Tokyo.

Conventional surface wind measurements, such as from ocean buoys, Doppler radar, drilling platforms and research vessels, are typically limited because of their sparse distribution; therefore, a wide range of observations is difficult to achieve. More importantly, while these traditional observation methodologies can measure ocean surface winds under low-to-moderate ocean conditions, they may become less accurate when wind speeds approach typhoon force. During the past 20 years, aircraft reconnaissance has been developed as perhaps the most accurate technology to acquire typhoon winds. In this approach, winds in typhoons are measured remotely using the Stepped-Frequency Microwave Radiometer (SFMR) on board the National Oceanic and Atmospheric Administration (NOAA) and Air Force Reserve typhoon research aircraft. The advantage of SFMR is that it can potentially provide along-track measurements of ocean surface winds, temperature and rain rates at relatively high spatial resolution (1.5 km), which are transmitted via satellite to the National Hurricane Center (Mueller et al., 2006). Unfortunately, because of cost and technical constraints, not all areas in the world are able to monitor typhoons using aircraft reconnaissance. This shortage has meant that forecasters and researches rely heavily on numerical weather predication (NWP) model data to investigate typhoon processes and mechanisms. Various advanced NWP models have significantly improved the forecasting of typhoon tracks during the last several decades (Montgomery and Smith, 2017). However, over the past two decades, no significant improvements have been made regarding the accuracy of typhoon intensity predictions. This remains challenging, despite recent efforts to develop enhanced informative observations, use advanced data assimilation methods, and apply more sophisticated modeling techniques (Alley et al., 2019; Jin et al., 2020).

With the development of satellite technology, the accuracy and reliability of ocean surface winds retrieved from spaceborne instruments has developed and improved, such as from radiometers, scatterometers, altimeters and synthetic aperture radars (SARs). Quick Scatterometer (QuickScat) and the advanced scatterometer (ASCAT) are designed to retrieve global sea surface wind at a resolution of 25 km twice a day. However, the accuracy of the retrieved wind data from scatterometers can be influenced by rain contamination and signal saturation (Chou et al., 2013). In comparison, spaceborne microwave SAR with its large area coverage, night and day imaging capability, and high spatial resolution (up to 1 m), is able to provide important measurements for typhoon winds, especially in areas over the sea where *in situ* measurements are sparse (Fang et al., 2018). Presently, ocean surface winds are routinely retrieved from co-polarized (VV, HH) SAR images using various geophysical model functions (GMFs), such as CMOD5, CMOD5.N and CMOD7 (Ren et al., 2019; Stoffelen et al., 2017). However, it has been reported that the normalized radar cross section (NRCS) values exhibit saturation for co-polarized SAR data, when wind speeds exceed about 15 $m \cdot s^{-1}$ (Hwang et al., 2015). Therefore, VV-polarized SAR images are often used to retrieve surface wind speeds under low-to-moderated sea conditions, rather than for typhoon forced conditions (Shen et al., 2016; Shao et al., 2018). In recent years, the cross-polarized (VH, HV) NRCS has been shown to be independent of wind direction and incidence angle, and to be quite linear with respect to sea surface wind speed, thereby providing a direct estimate of wind speed (Zhang et al., 2014). More importantly, the measured backscatters for cross-polarized SAR data seem almost not to become saturated, even at very high winds speeds ($> 50\ m \cdot s^{-1}$); this suggests that the latter can potentially be used to investigate winds in typhoons (Deng et al., 2017; Gao et al., 2019). Currently, several cross-polarized GMFs have been developed to retrieving typhoon winds, i.e., C-2POD (Zhang et al., 2014), VH + ECMWF (van Zadelhoff et al., 2014), dual-pol GMF (Shen et al., 2016) and C-3PO (Zhang et al., 2017a). These empirical models have been successfully applied to typhoon intensity retrieval in the North Pacific and North Atlantic Oceans.

Presently available SAR wind retrieval models have been developed for a broad list of satellites, such as the Canada's RADARSAT – 1/2, European Space Agency Advanced SAR (ASAR) and Sentinel – 1. On 10 August 2016, the first Chinese spaceborne multi-polarization SAR was launched by the China Academy of Space Technology. This is a C-band (5.43GHz) SAR named Gaofen-3 (GF-3). After over four years of operation, the GF-3 SAR has acquired a large quantity of global data; several studies have used this data for ocean surface wind monitoring. Wang et al. (2017) selected 56 pairs of collocations of GF-3 images with buoy-measured winds to preliminarily evaluate the quality of surface wind retrieval; the results show a root mean square error (RMSE) of 2.46 $m \cdot s^{-1}$. Ren et al. (2019) conducted a more detailed analysis of surface wind retrieval from GF-3, using quad-polarized data at VV, HH and HV channels. Regarding typhoon intensity monitoring, the first GF-3 SAR image of a typhoon was acquired at 21:24 UTC on August 4, 2107 and covered Typhoon Noru in the Northwest Pacific area (Lin et al., 2017). Recently, Zhang et al. (2019) have retrieved ocean surface wind speed under Typhoon Soulik (2018) using a GF-3 wide ScanSAR(WSC) VH-polarized image. Their results show good agreement between the SAR-retrieved wind speeds and collocated NWP model winds from the

Global Forecast System (GFS) model. However, it is still uncertain about the performance of GF-3 SAR under super Typhoon condition.

Super Typhoon Lekima (2019), with the maximum wind speed 62 $m \cdot s^{-1}$ at 12:00 UTC on 8 August, made landfall at the city of Wenling in Zhejiang Province on 10 August. Fortunately, the Chinese GF-3 SAR successfully observed Lekima in the East China Sea at 21:56:59 UTC on August 2019, using wide ScanSAR (WSC) mode with spatial resolution of 100 m and a swath width of 500 km (Fig. 1(b)). The storm track and entire life of Super Typhoon Lekima (2019) are shown in Fig.1(a), from 06:00 Universal Time Coordinated UTC (4 August) to 03:00 UTC (13 August). In this paper, we will obtain the high-resolution sea surface winds of Super Typhoon Lekima (2019) based on the Gaofen-3 SAR, and further make a detailed evaluation using buoy-measured and numerical model data. Datasets and methods are described in Section 2, results and discussion are given in Section 3, and finally, conclusions are given in Section 4.

2 Datasets and methods

2.1 GF-3 SAR data and wind retrieval algorithm

The first Chinese spaceborne multi-polarization SAR at C-band (5.43 GHz), named Gaofen-3 (GF-3), was launched by China Academy of Space Technology on 10 August 2016. The GF-3 SAR has 12 imaging modes, which is as many as any existing SAR formulation. Among these imaging modes, the Wide ScanSAR (WSC) modes are very suitable for typhoon monitoring and wind field retrieval, since they provide a swath width larger than 500 km. This advantage has been exploited to observe typhoons over the China Seas from 2017 to 2019 (Lin et al., 2017; Shao et al., 2019). In this paper, we focus on a GF-3 WSC mode image for Super Typhoon Lekima (2019) that was acquired on 8 August 2019, at 21:56:59 UTC. This SAR image has a medium spatial resolution of 100 m and a swath width of 500 km. The incidence angles range from 14° to 41°.

Preprocessing of the raw SAR data is essential for accurate sea surface wind retrieval. Therefore, before retrieving wind speed from GF-3 SAR image, we first convert the raw SAR backscatter signal into calibrated NRCS, based on the following relation:

$$\sigma^0_{\mathrm{VH}} = DN^2 \left(\frac{M}{65535} \right) - N, \tag{1}$$

where the σ^0_{VH} is the VH-polarized NRCS, DN is the SAR pixel intensity, M is the external calibration coefficient and N is the offset factor for a specific imaging mode. Subsequently, we averaged the spatial resolution to 1000 m with the boxcar averaging method, to reduce the speckle noise (Shen et al., 2014; Zhang, et al., 2017a). Finally, in order to eliminate the effect of coastal islands on NRCS, a-10 m water depth contour was applied to mask these islands and coastal lands from the SAR image.

Based on a GF-3 WSC VH-polarized SAR image, which is similar to the data used in our present study, Zhang et al. (2019) previously retrieved the ocean surface wind speed using the QPS-CP model for Typhoon Soulik (2018). Their results show that the SAR-retrieved wind speeds are in good agreement with the GFS wind speed. This indicates the feasibility of using the QPS-CP model for wind speed retrieval at high wind conditions for GF-3 VH-polarized

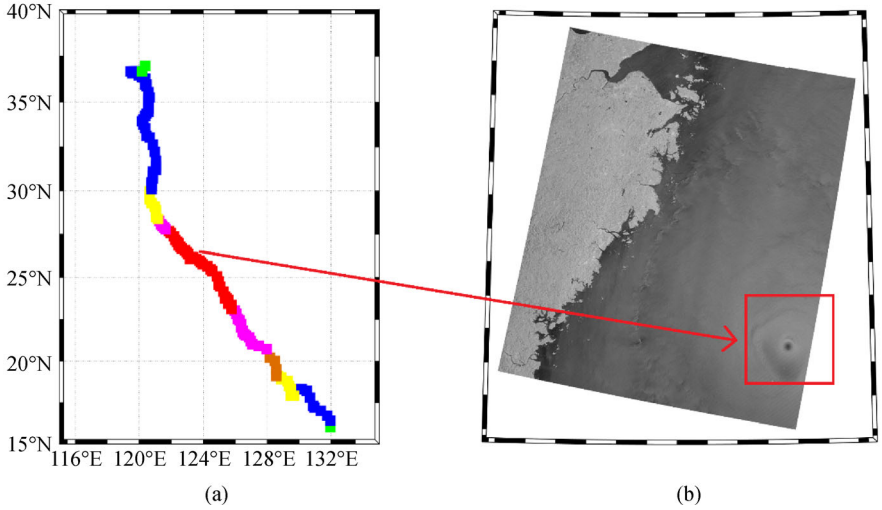

Fig. 1 (a) The track and entire life of Super Typhoon Lekima (2019) according to the best-track in China Meteorological Administration. The green, blue, yellow, orange, purple, and red colors represent its different phases as a tropical depression, tropical storm, severe tropical storm, typhoon, severe typhoon and super typhoon, respectively; (b) collocated GF-3 SAR raw image using VH-polarized mode over the East China Sea on 8 August 2019, at 21:56:59 UTC. The red square represents the typhoon center area.

SAR data. Thus, we selected the QPS-CP model here, to retrieve wind speed from the GF-3 SAR image for Typhoon Lekima. The QPS-CP model is given by the follow equation:

$$\sigma^0_{\mathrm{VH}} = 0.4273U_{10} - 34.3875, \tag{2}$$

where σ^0_{VH} is the NRCS in VH polarization, U_{10} is the ocean surface wind speed at 10-m reference height.

2.2 *In situ* buoys

Buoy-measured wind speeds are generally assumed to be of high quality, even in extreme sea conditions, and hence can be taken as 'ground truth' for validation of wind retrieval from GF-3 SAR. In this paper, we obtained *in situ* wind observations from seven China State Oceanic Administration (SOA) buoys and five Zhejiang Meteorological Administration (ZMO) buoys in the East China Sea area. These are compared to wind measurements from the collocated GF-3 SAR image. Figure 3(a) shows the buoy locations within the SAR image. These moored buoys provide winds are measured 10-min by averaging the wind direction and wind speed. Therefore, the temporal separation between the SAR image and buoy data is restricted to less than 10 min. Since the anemometers on the buoys are at different heights above the ocean surface, buoy-measured wind speeds need to be converted to values at 10 m reference height for comparison with SAR-retrieved winds. We assume neutral winds. The correction was performed using the following wind profile algorithm (Wang et al., 2017):

$$u(z) = \frac{\mu}{\kappa}\ln\left(\frac{z}{z_0}\right), \tag{3}$$

where $\kappa = 0.4$ is the von Kármán constant, $u(z)$ is the sea surface wind speed at height z, μ is the friction velocity, which is related to the ocean surface roughness length z_0 by Leite et al. (2010):

$$z_0 = \frac{0.11\nu}{\mu} + \frac{\zeta\mu^2}{\mathrm{g}} \tag{4}$$

where $\nu = 1.5\times10^{-5}\mathrm{m\cdot s^{-2}}$ is the kinematic viscosity of air, $\zeta = 0.011$ is the Charnock parameter and g is the gravitational acceleration.

2.3 NWP model data

NWP (numerical weather prediction) model products are constructed by using a weather model, weather observations and applying a data assimilation process to forecast the future state of weather (Jin et al., 2020). We use two common NWP products to analyze surface winds under Super Typhoon Lekima (2019): 1) European Centre for Medium-Range Weather Forecasts (ECMWF) fine grid operational forecast products with 0.125° spatial resolution, and 2) China Global/Regional Assimilation and Prediction Enhance System (GRAPES) high-resolution regional forecast products with 0.25º spatial resolution. These two model systems can provide consistent and credible forecasts of wind components U (west-east direction) and V (north-south direction) at 10-m height above the sea surface every 3-hours. The two model systems are run twice daily, out of a lead time of 10 days, with initial times at 0000 and 1200UTC.

2.4 Spatial and temporal interpolation

Comparison of buoy observations, SAR measurements and NWP products (ECMWF and GRAPES) require the matching of buoy wind values, and SAR and NWP winds, in both space and time. In terms of time, we require that surface wind speeds from buoys, NWP products and SAR data fall within 30 min of one another. In terms of space, because the spatial resolution of the NWP model systems are not the same as that of the SAR image, only the NWP grid cells located within the SAR image are considered as co-located in space. Therefore, a space matching algorithm is used to identify NWP model data that are located within the SAR scene. Fig. 2 shows the general flowchart for the space matching algorithm. Taking the GRAPES model system as an example, the GRAPES wind data are available at 0.25º×0.25º resolution, whereas SAR imagery has a wide swath of 500 km implying that there are 75 possible matchups available to study the relation between GRAPES winds and SAR measurements (see Fig. 3(b)). Moreover, because the GRAPES grid cells and SAR pixels are usually misaligned, we use bilinear

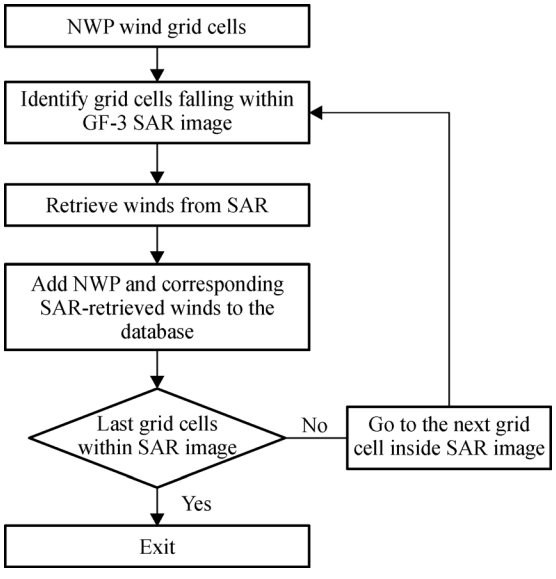

Fig. 2 Flowchart of the space matching algorithm between NWP models and the SAR image.

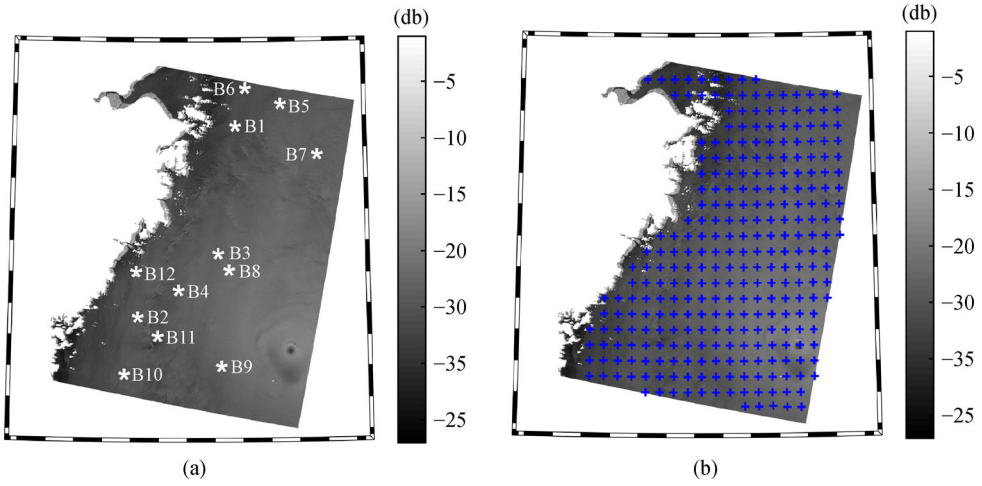

Fig. 3 (a) *In situ* buoy locations and (b) GRAPES model system grid cells falling within the SAR image. White '*' denotes buoys and blue '+' represents GRAPES model data.

interpolation in order to obtain the SAR-derived winds at the GRAPES grid cells (Komarov et al., 2014). These selected measurements can be treated as being essentially independent. Available match-up pairs among buoys, NWP models and the SAR image are indicated in Table 1.

3 Results and discussion

3.1 Overview of Super Typhoon Lekima (2019)

Super Typhoon Lekima formed as a tropical depression to the east of Luzon, Philippines, on 4 August 2019. It strengthened as a tropical storm at 09:00 UTC on 4 August, and soon intensified to a typhoon on the evening of 6 August. Lekima upgraded to a super typhoon at 14:00 UTC on 7 August, with minimum sea level pressure of 930 hPa and maximum ocean surface winds of 52 $m \cdot s^{-1}$. After 7 August, Lekima's convective processes strengthened gradually, and its intensity continued to gradually increase. On 8−10 August, Lekima arrived at the East China Sea area with maximum winds of 62 $m \cdot s^{-1}$ and minimum sea level pressure of 920 hPa. The China Meteorological Administration issued an offshore and coastal typhoon warning. Lekima made landfall at Wenling City, Zhejiang Province, at 09:45 UTC on 10 August, with maximum winds of 52 $m \cdot s^{-1}$, arriving at Shanghai at 08:00 UTC on 11 August 2019. Crossing Jiangsu Province on 10 August 2019, it moved to Shandong Province and the adjacent waters, where Lekima experienced further decline to an extratropical cyclone.

3.2 GF-3 surface winds retrieval and validation

The two-dimensional wind field obtained from the VH-polarized SAR data is shown in Fig. 4, based on the QPS-CP wind speed retrieval model introduced in Section 2. Because of the high spatial resolution of the SAR image, the retrieved wind field clearly shows the structure of Typhoon Lekima, particularly the intense winds of the eyewall. These suggest a maximum sea surface wind speed, $V_{\max}^{\mathrm{SAR}}$, of 38.9 $m \cdot s^{-1}$. This is notable because such eyewall wind structure is usually underestimated by winds retrieved from VV-polarized SAR images, especially when the eyewall is located in the low incidence angle area of the SAR image where the VV-polarized SAR NRCS suffers signal saturation leading to the wind speed ambiguity phenomenon (Shen et al., 2014; Zhang et al., 2017b). Figure 4 also indicates smaller VH-NRCS values associated with lower winds in the typhoon eye area, and larger VH-NRCS values related to higher winds in the eyewall region. It is interesting that a local wind minimum occurs to the south of the eyewall, separating an outer wind maximum from the eyewall. This may be related to its concentric eyewall structure (Zhu and Yu, 2016; Zhu et al., 2019).

In order to validate the retrieved wind speeds, we interpolated SAR-measured winds to the *in situ* buoy location using bilinear interpolation. Here, *RMSE*, bias and correlation coefficient (correlation coefficient) are computed as

$$RMSE = \sqrt{\frac{1}{M}\sum_{i=1}^{M}(X_i - Y_i)^2}, \tag{5}$$

$$\text{bias} = \frac{1}{M}\sum_{i=1}^{M}(X_i - Y_i), \tag{6}$$

$$\text{correlation coefficient} = \frac{\text{cov}(X,Y)}{|Y|}, \tag{7}$$

where X and Y are the SAR-retrieved wind speed and buoy

Table 1 Detailed information on data subset on 8 August, 2019

Data subset	Acquired time (UTC)	Spatial resolution	Grid cells in SAR
GF-3 SAR	21:56:59	1 km×1 km	/
Buoys	21:30	/	12
GRAPES	21:00:00	0.25°×0.25°	278
ECMWF		0.125°×0.125°	1028

measurements, respectively. Note that in the following Section 3.2, X denotes the wind speed from the buoy observations and SAR image and Y denotes NWP model wind data. Here, M is the total number of the collocated data inside the SAR image as shown in Table 1.

As can be seen in Fig. 3(a), most buoys locate far away from typhoon circulation. Therefore, we first evaluate the GF-3 SAR retrieved background wind of Typhoon Lekima with the available buoy measurements (Fig. 3(a)). Figure 5 shows the scatterplot for the comparisons between the SAR retrieved wind and buoy measurements; additional information is given in Table 2. As can be seen from the scatter diagram, wind speeds retrieved from the SAR image are in good agreement with buoy measurements, with RMSE of 1.86 m·s^{-1} and correlation coefficient of 0.92. These results suggest that background wind speeds retrieved from the GF-3 SAR image are reliable.

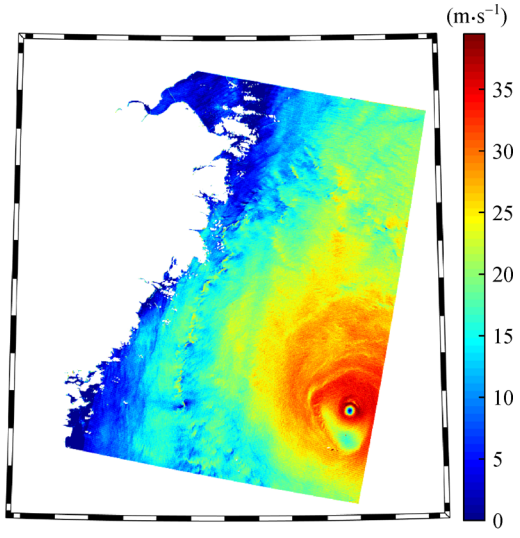

Fig. 4 Ocean surface wind speed retrieved from the GF-3 SAR image using the QPS-CP model at VH-polarization for Super Typhoon Lekima (2019).

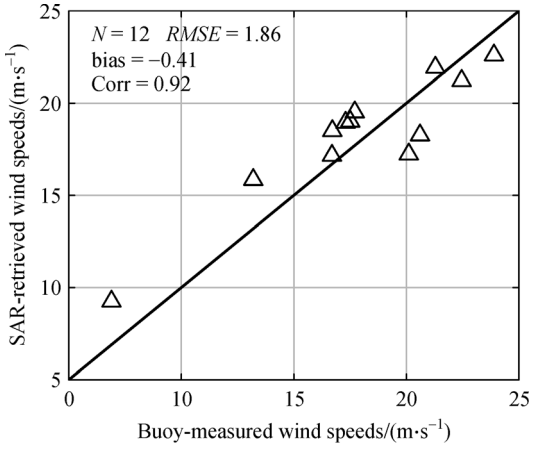

Fig. 5 Ocean surface wind speeds retrieved from the GF-3 SAR image vs *in situ* buoy measurements.

3.3 Comparisons between SAR winds and NWP model estimates

Although NWP models have made significant advances in forecasting ocean surface wind speeds in typhoons, the verification of these winds, and concomitant predictions of typhoon intensity, are still important questions because of the lack of *in situ* data and the reliance on satellite observations. Figure 6 shows the ocean surface wind maps from ECMWF and GRAPES products overlaid with the SAR spatial coverage on 8 August at 21:00; this is the model output time that is nearest to the SAR imaging time.

Table 2 Wind speed retrieved from GF-3 SAR image compared with buoy measurements (unit: m·s^{-1})

Buoy ID	Buoy wind	SAR wind	Bias	Buoy ID	Buoy wind	SAR wind	Bias
B1	13.2	15.84	2.64	B7	17.5	19.01	1.51
B2	20.11	17.23	2.88	B8	21.3	21.91	0.61
B3	22.45	21.21	1.24	B9	23.9	22.58	1.32
B4	20.61	18.26	2.35	B10	17.7	19.51	1.81
B5	16.7	18.51	1.81	B11	17.3	18.95	1.65
B6	6.64	8.95	2.31	B12	16.7	17.15	0.45

Although ECMWF and GRAPES models have different spatial resolutions, the forecast winds indicate a powerful storm with a clear, well-developed eye structure, and intense ocean surface wind speeds in the typhoon area. However, the magnitude of the wind speeds is quite different from that of the SAR-retrieved winds shown in Fig. 4, especially the peak winds. Specifically, the maximum winds from ECMWF ($V_{\max}^{\mathrm{ECMWF}}$) and GRAPES ($V_{\max}^{\mathrm{GRAPES}}$) are 31.03 $\mathrm{m\cdot s^{-1}}$ and 33.47 $\mathrm{m\cdot s^{-1}}$, respectively, within the spatial area covered by the SAR image, whereas the peak SAR-retrieved wind is 38.9 $\mathrm{m\cdot s^{-1}}$. This result suggests that the ECMWF and GRAPES models underestimate the wind speeds for Super Typhoon Lekima (2019). Moreover, this result is consistent with similar findings by Magnusson et al. (2019), comparing maximum wind speeds in ECMWF forecasts of tropical cyclones to analysis results from BestTrack data.

Because all buoy locations are relatively distant from the typhoon center area, the maximum wind speed for *in situ* buoy measurements is only 23.9 $\mathrm{m\cdot s^{-1}}$ (buoy B9). Therefore, it is necessary to assess the performance of the NWP models with respect to SAR-retrieved winds, since *in situ* buoy observations are not available for high wind conditions. Usually, the 2-min mean MWS defines the typhoon's intensity. When the MWS greater than 24.4 $\mathrm{m\cdot s^{-1}}$ and less than 32.6 $\mathrm{m\cdot s^{-1}}$, it is named and tracked as a "severe tropical storm" (Zhong et al., 2020). Therefore, we take 24.4 $\mathrm{m\cdot s^{-1}}$ as the wind speed threshold defining severe tropical storm intensity, to analyze NWP model winds and SAR-retrieved winds. Figures. 7(a) and 7(b) compare the NWP models wind speeds and SAR-retrieved measurements for winds in the range 0–24.4 $\mathrm{m\cdot s^{-1}}$. Both NWP models show good agreement with the SAR measurements. With respect to SAR-retrieved wind speeds, the RMSEs are 2.45 $\mathrm{m\cdot s^{-1}}$ for ECMWF, and 2.72 $\mathrm{m\cdot s^{-1}}$ for GRAPES; the correlation coefficients are 0.86 for ECMWF and 0.85 for GRAPES. In terms of RMSE, the ECMWF model slightly outperforms the GRAPES model for Lekima, for 0−24.4 $\mathrm{m\cdot s^{-1}}$ winds.

Results for winds greater than 24.4 $\mathrm{m\cdot s^{-1}}$ are shown in Figs. 7(c) and 7(d). These results clearly suggest that both ECMWF and GRAPES models underestimate winds when they are great than 24.4 $\mathrm{m\cdot s^{-1}}$. With respect to SAR-retrieved wind speeds, the RMSEs are 5.24 $\mathrm{m\cdot s^{-1}}$ for ECMWF and 5.17 $\mathrm{m\cdot s^{-1}}$ for GRAPES; corresponding biases are 4.16 $\mathrm{m\cdot s^{-1}}$ for ECMWF and 3.84 $\mathrm{m\cdot s^{-1}}$ for GRAPES.

4 Conclusions

In this paper, wind data from the satellite-borne GF-3 SAR, two NWP model systems and several *in situ* ocean buoys, are compared in order to investigate and analyze ocean surface winds during Super Typhoon Lekima (2019) in the East China Sea. A space matching algorithm was used to identify NWP models grid cells that are located within the SAR image, in order to compare these wind data at given locations.

In order to evaluate wind retrieval accuracy from the VH-polarized SAR image, the wind speeds measured from *in situ* buoys are used as reference data. Results show that SAR-retrieved wind speeds have good agreement with buoy-measured winds, with *RMSE* of 1.86 $\mathrm{m\cdot s^{-1}}$ and correlation coefficient of 0.92. This suggests that wind speeds retrieved from the GF-3 SAR image are reliable. They also have high spatial resolution. Subsequently, the SAR-retrieved wind speeds were taken as reference data in order to validate the performance of two different models, ECMWF and GRAPES, since *in situ* buoy observations of high wind conditions are not available during Typhoon

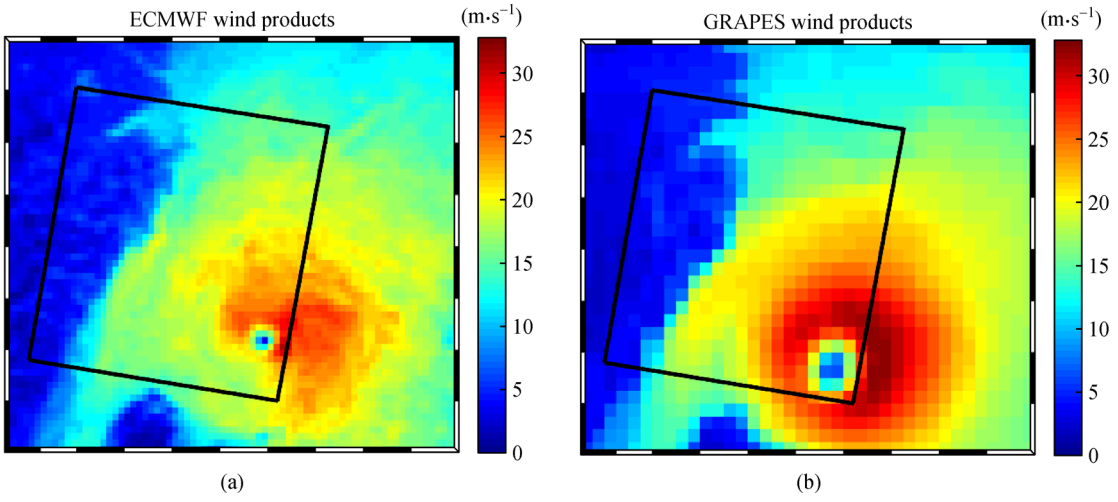

Fig. 6 (a) ECMWF and (b) GRAPES model winds under Super Typhoon Lekima (2019) on 8 August at 21:00 UTC. The black boxes show the GF-3 footprint related to the scene collected at 21:56:59 UTC.

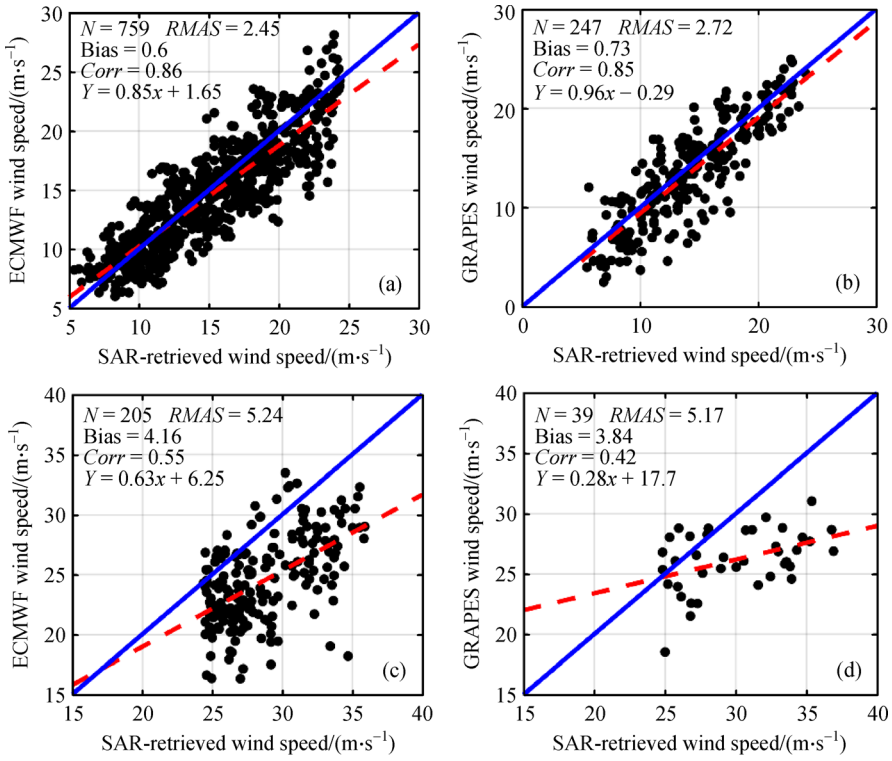

Fig. 7 SAR-retrieved wind speeds from the SAR image versus (a) ECMWF and (b) GRAPES models for 0–24.4 $m \cdot s^{-1}$ winds, and (c) ECMWF and (d) GRAPES models for winds greater than 24.5 $m \cdot s^{-1}$.

Lekima. Results shows that ECMWF and GRAPES models have good agreement with SAR measurements for winds in the range 0–24.4 $m \cdot s^{-1}$, with RMSE of 2.45 $m \cdot s^{-1}$ for ECMWF and 2.72 $m \cdot s^{-1}$ for GRAPES. However, for winds above 24.4 $m \cdot s^{-1}$, we find that ECMWF and GRAPES models underestimate the wind speeds, with a bias of 4.16 $m \cdot s^{-1}$ for ECMWF and 3.84 $m \cdot s^{-1}$ for GRAPES.

Advanced spaceborne techniques for observing ocean surface wind field with high spatial resolution (up to 1 m) from SAR measurements present unique advantages, providing wind data over areas lacking *in situ* ground measurements from buoys or other instruments. Moreover, satellite observations presently contribute to most of the error reduction in forecasts. In further studies, a constellation of satellites is needed to improve the prediction skill for typhoon intensities, and to provide better understanding of the typhoon formation mechanisms. These could include the Chinese GF-3 SAR instrument, in conjunction with other SAR satellites, such as the Canadian RADARSAT-2 and three RADARSAT Constellation Mission satellites, and the European Space Agency Sentinel－1 satellite.

Acknowledgements This work was supported in part by the Natural Science Foundation of Zhejiang Province (No. LQ21D060001), the Fengyun Application Pioneering Project (No. FY-APP-2021.0105), the Science and Technology Project of Zhejiang Meteorological Bureau (No. 2021YB07), the Innovation and Development Project of China Meteorological Administration (No. CXFZ2022J040), the National Key R&D Program of China (No. 2018YFC1506404), the Basic Public Welfare Research Program of Zhejiang Province (No. LGF18D050001), the Climate Change Special Program of China Meteorological Administration (No. CCSF202036), the Key Research and Development Program of Zhejiang Province (No. 2021C02036), the Research Program from Science and the Technology Committee of Shanghai (No.19dz1200101), the Shanghai Typhoon Institute (No. 2021JB05), and the open fund of State Key Laboratory of Satellite Ocean Environment Dynamics, Second Institute of Oceanography, MNR (No. QNHX2012).

References

Alley R B, Emanuel K A, Zhang F (2019). Advances in weather prediction. Science, 363(6425): 342–344

Buchanan S, Misra V, Bhardwaj A (2018). Integrated kinetic energy of Atlantic tropical cyclones in a global ocean surface wind analysis. Int J Climatol, 38(6): 2651–2661

Cangialosi J P, Kimberlain T B, Beven J L II, Demaria M (2015). The validity of dvorak intensity change constraints for tropical cyclones. Weather Forecast, 30(4): 1010–1015

Chou K H, Wu C C, Lin S Z (2013). Assessment of the ASCAT wind error characteristics by global dropwindsonde observations. J Geophys Res Atmos, 118(16): 9011–9021

Deng M, Zhang G, Zhao R, Li S, Li J (2017). Improvement of gaofen-3 absolute positioning accuracy based on cross-calibration. Sensors (Basel), 17(12): 2903

Fang H, Xie T, Perrie W, Zhang G, Yang J, He Y (2018). Comparison of C-band quad-polarization synthetic aperture radar wind retrieval models. Remote Sens, 10(9): 1448

Gao Y, Guan C, Sun J, Xie L (2019). A wind speed retrieval model for Sentinel-1A EW mode cross-polarization images. Remote Sens, 11 (2): 153

Hwang P A, Stoffelen A, van Zadelhoff G J, Perrie W, Zhang B, Li H, Shen H (2015). Cross-polarization geophysical model function for C-band radar backscattering from the ocean surface and wind speed retrieval. J Geophys Res Oceans, 120(2): 893–909

Huang X, Peng X, Fei J, Cheng X, Ding J, Yu D (2021). Evaluation and error analysis of official tropical cyclone intensity forecasts during 2005–2018 for the western North Pacific. J Meteorol Soc Jpn, 99

Jin Q, Fan X, Liu J, Xue Z, Jian H (2020). Estimating tropical cyclone intensity in the South China Sea using the XGBoost Model and FengYun Satellite images. Atmosphere, 11(4): 423

Komarov A S, Zabeline V, Barber D G (2014). Ocean surface wind speed retrieval from C-band SAR images without wind direction input. IEEE Trans Geosci Remote Sens, 52(2): 980–990

Leite G C, Ushizima D M, Medeiros F N S, de Lima G G (2010). Wavelet analysis for wind fields estimation. Sensors (Basel), 10(6): 5994–6016

Lin M, Ye X, Yuan X (2017). The first quantitative joint observation of typhoon by Chinese GF-3 SAR and HY-2A microwave scatterometer. Acta Oceanol Sin, 36(11): 1–3

Magnusson L, Bidlot J R, Bonavita M, Brown A R, Browne P A, De Chiara G, Dahoui M, Lang S T K, McNally T, Mogensen K S, Pappenberger F, Prates F, Rabier F, Richardson D S, Vitart F, Malardel S (2019). ECMWF activities for improved hurricane forecasts. Bull Am Meteorol Soc, 100(3): 445–458

Montgomery M T, Smith R K (2017). Recent developments in the fluid dynamics of tropical cyclones. Annual Review of Fluid Mechanics, 49: 541–574

Mueller K J, DeMaria M, Knaff J, Kossin J P, Vonder Haar T H (2006). Objective estimation of tropical cyclone wind structure from infrared satellite data. Weather Forecast, 21(6): 990–1005

Ren L, Yang J, Mouche A A, Wang H, Zheng G, Wang J, Zhang H, Lou X, Chen P (2019). Assessments of ocean wind retrieval schemes used for Chinese gaofen-3 synthetic aperture radar co-polarized data. IEEE Trans Geosci Remote Sens, 57(9): 7075–7085

Sangster S J, Landsea C W (2020). Constraints in dvorak wind speed estimates: how quickly can hurricanes intensify? Weather Forecast, 35(4): 1235–1241

Shao W, Ding Y, Li J, Gou S, Nunziata F, Yuan X, Zhao L (2019). Wave retrieval under typhoon conditions using a machine learning method applied to Gaofen-3 SAR imagery. Can J Rem Sens, 45(6): 723–732

Shao W, Yuan X, Sheng Y, Sun J, Zhou W, Zhang Q (2018). Development of wind speed retrieval from cross-polarization Chinese gaofen-3 synthetic aperture radar in typhoons. Sensors (Basel), 18(2): 412–427

Shen H, Perrie W, He Y (2016). Evaluation of hurricane wind speed retrieval from cross-dual-pol SAR. Int J Remote Sens, 37(3): 599–614

Shen H, Perrie W, He Y, Liu G (2014). Wind speed retrieval from VH dual-polarization RADARSAT-2 SAR Images. IEEE Trans Geosci Remote Sens, 52(9): 5820–5826

Stoffelen A, Verspeek J A, Vogelzang J, Verhoef A (2017). The CMOD7 geophysical model function for ASCAT and ERS wind retrievals. IEEE J Sel Top Appl Earth Obs Remote Sens, 10(5): 2123–2134

Uhlhorn E W, Klotz B W, Vukicevic T, Reasor P D, Rogers R F (2014). Observed hurricane wind speed asymmetries and relationships to motion and environmental shear. Mon Weather Rev, 142(3): 1290–1311

Wang H, Yang J, Mouche A, Shao W, Zhu J, Ren L, Xie C (2017). GF-3 SAR oceanwind retrieval: the first view and preliminary assessment. Remote Sens, 9(7): 694–706

van Zadelhoff G J, Stoffelen A, Vachon P W, Wolfe J, Horstmann J, Belmonte Rivas M (2014). Retrieving hurricane wind speeds using cross-polarization C-band measurements. Atmos Meas Tech, 7(2): 437–449

Zhang B, Perrie W, Zhang J A, Uhlhorn E W, He Y (2014). High-resolution hurricane vector winds from C-band dual-polarization SAR observations. J Atmos Ocean Technol, 31(2): 272–286

Zhang G, Li X, Perrie W, Hwang P A, Zhang B, Yang X (2017a). A hurricane wind speed retrieval model for C-band RADARSAT-2 cross-polarization ScanSAR images. IEEE Trans Geosci Remote Sens, 55(8): 4766–4774

Zhang G, Perrie W, Li X, Zhang J A (2017b). A hurricane morphology and sea surface wind vector estimation model based on C-band cross-polarization SAR imagery. IEEE Trans Geosci Remote Sens, 55(3): 1743–1751

Zhang T, Li X M, Feng Q, Ren Y, Shi Y (2019). Retrieval of sea surface wind speeds from Gaofen-3 full polarimetric data. Remote Sens, 11 (7): 813

Zhong R, Xu S, Huang F, Wu X (2020). Reasons for the weakening of tropical depressions in the South China Sea. Mon Weather Rev, 148 (8): 3453–3469

Zhu X S, Yu H, Mao Z C, Xu M, Tan J G (2016). Satellite-based analysis on the concentric eyewall replacement cycles of super Typhoon Muifa (1109). J Trop Meteorol, 22: 330–340

Zhu X S, Yu H (2019).Environmental influences on the intensity and configuration of tropical cyclone concentric eyewalls in the western North Pacific. J Meteor Soc Japan, 97: 153–173